REVIEW
PHYSIOLOGY 32: 346–356, 2017. Published August 16, 2017; doi:10.1152/physiol.00040.2016

Right Ventricular-Pulmonary Vascular Interactions

Diana M. Tabima,[1]* Jennifer L. Philip,[1,2]* and Naomi C. Chesler[1]

[1]Department of Biomedical Engineering, University of Wisconsin-Madison College of Engineering, Madison, Wisconsin; and [2]Department of Surgery, University of Wisconsin-Madison, Madison, Wisconsin
*D. M. Tabima and J. L. Philip contributed equally to this work.
Naomi.Chesler@wisc.edu

Accurate and comprehensive evaluation of right ventricular (RV)-pulmonary vascular (PV) interactions is critical to the assessment of cardiopulmonary function, dysfunction, and failure. Here, we review methods of quantifying RV-PV interactions and experimental results from clinical trials as well as large- and small-animal models based on pressure-volume analysis. We conclude by outlining critical gaps in knowledge that should drive future studies.

The function of the right ventricular-pulmonary vascular unit depends on the function of its components as well as the dynamics of their interactions. A framework for understanding these interactions is the relationship between supply and demand. In a healthy state, the supply of blood pressure and blood flow is adequate to meet demand; increases in demand, such as generated by exercise, changes in altitude, or increased blood volume in pregnancy, are met by increases in supply. However, in disease states such as pulmonary arterial hypertension (PAH), which progresses from first symptoms to death in 5 yr for 55% of patients (82), increases in demand cannot be met by increases in supply, with right ventricular failure the consequence. Using this framework, here we review investigations of right ventricular-pulmonary vascular interactions, results from their use in preclinical and clinical studies, and conclude with suggestions for future work.

Supply and Demand: A Framework to Assess Right Ventricular-Pulmonary Vascular Interactions

Cardiopulmonary status is determined by the state of the right ventricle (RV), the pulmonary vasculature (PV), and their interactions, assuming adequate respiratory function. The RV-PV unit can be conceptualized as a series of pumps, which supply mechanical energy, and a network of large and small pipes, which simultaneously demand and dissipate this energy. Hemodynamically, RV energy supply is created by RV myocyte contraction, which depends on the preload (stretch), afterload (stress) imposed, and bioenergetics status (e.g., oxygen bioavailability, mitochondrial function, ATP levels, etc.). Moreover, RV pump function depends on left ventricular (LV) pump function; it has been estimated that 20–40% of RV energy supply (systolic pressure and volume outflow) is due to LV ejection in a healthy state (19, 30, 69). Hemodynamic energy demand in this framework is the cardiac output, largely determined by the LV and systemic vasculature, and transformed by the pulmonary vasculature. In particular, pulmonary vascular resistance and stiffness (inverse compliance) create a mean and pulse pressure demand from the cardiac output (flow demand); here, we denote the combination as PV demand (FIGURE 1).

Given this framework, methods to simultaneously assess RV supply and PV demand are essential to evaluation of RV-PV interactions. One such approach was proposed by Sagawa et al. for left ventricular-systemic vascular interactions based on pressure-volume (P-V) loops (FIGURE 2) (68). In P-V analysis, the ventricle is conceptualized as a sac that has a time-varying stiffness or elastance due to myocardial contraction and relaxation. Beginning at the start of isovolumic contraction, the elastance increases from an initial minimum to a peak value (E_{max}), and then returns to the minimum value again. The instantaneous elastance $E(t)$ is defined mathematically as $E(t) = P(t)/[V(t) - V_0]$, where $P(t)$ is the instantaneous pressure, $V(t)$ is the instantaneous volume, and V_0 is the volume intercept of the line connecting the P-V points at the same phase of the cardiac cycle at two (or more) different preload conditions (17, 48, 67, 68, 95) (FIGURE 2). Although V_0 can change with time (68), it is often assumed constant and equal to the value obtained at end systole (FIGURE 2).

Because it can be difficult to identify E_{max} from P-V curves, it is typically assumed equal to the end-systolic elastance (E_{es}) determined from a linear approximation to the end-systolic P-V relationship (ESPVR) (FIGURE 2). Although this approach is recommended by most experts (90), some accuracy is lost when ESPVR is assumed to be linear, since it is inherently curvilinear and typically convex to the pressure axis (11, 34). E_{es} is a commonly used load-independent measure of contractility that can be derived from P-V loops, but it is affected by changes in heart rate (52), reduction in coronary perfusion pressure (74), and ionotropic state (48).

When E_{es} is used to define hemodynamic energy supply, a complementary elastance of the vasculature is used to compute hemodynamic energy demand: the effective arterial elastance (E_a) is the slope of the line that connects the ventricular end-systolic point to the ventricular end-diastolic volume projected on the volume axis (FIGURE 2). E_a is a composite measure that is dependent on vascular resistance and compliance. It has the advantage (and disadvantages) of being a single metric of ventricular afterload. One disadvantage is that, like E_{es}, it is dependent on heart rate (73, 75).

The ratio of ventricular to vascular elastance (E_{es}/E_a), yields insight into the balance between hemodynamic energy supply and demand in the ventricular-vascular unit. It also provides a quantitative assessment of the adequacy of ventricular-vascular coupling (VVC). Experimental and modeling studies have demonstrated that, in the healthy beating heart, E_{es}/E_a = 1.5–2.0. Despite these healthy values of >1, E_{es}/E_a is often referred to as ventricular-vascular coupling efficiency. In a mechanical system, efficiency is defined as the ratio of output power to input power; transmission of power is maximized when the output impedance of the power-producing part and the input impedance of the power-receiving part are equal such that the efficiency of the system is equal to one. When energy dissipation occurs, efficiency is <1. Calculating an equivalent efficiency of the ventricular-vascular unit would require measurement of input power or energy (e.g., oxygen consumption), and output power or energy (e.g., stroke work), which is challenging and thus infrequently done (10, 41).

The application of P-V loop analysis to the RV-PV unit was validated by Maughan and collaborators (48) with studies in isolated canine hearts. Clinical application of RV P-V loop analysis, often with significant approximations (as described below), has shown that lower values of E_{es}/E_a predict mortality in PAH (3, 8, 32, 44, 59). Higher values of E_{es}/E_a have been interpreted to mean

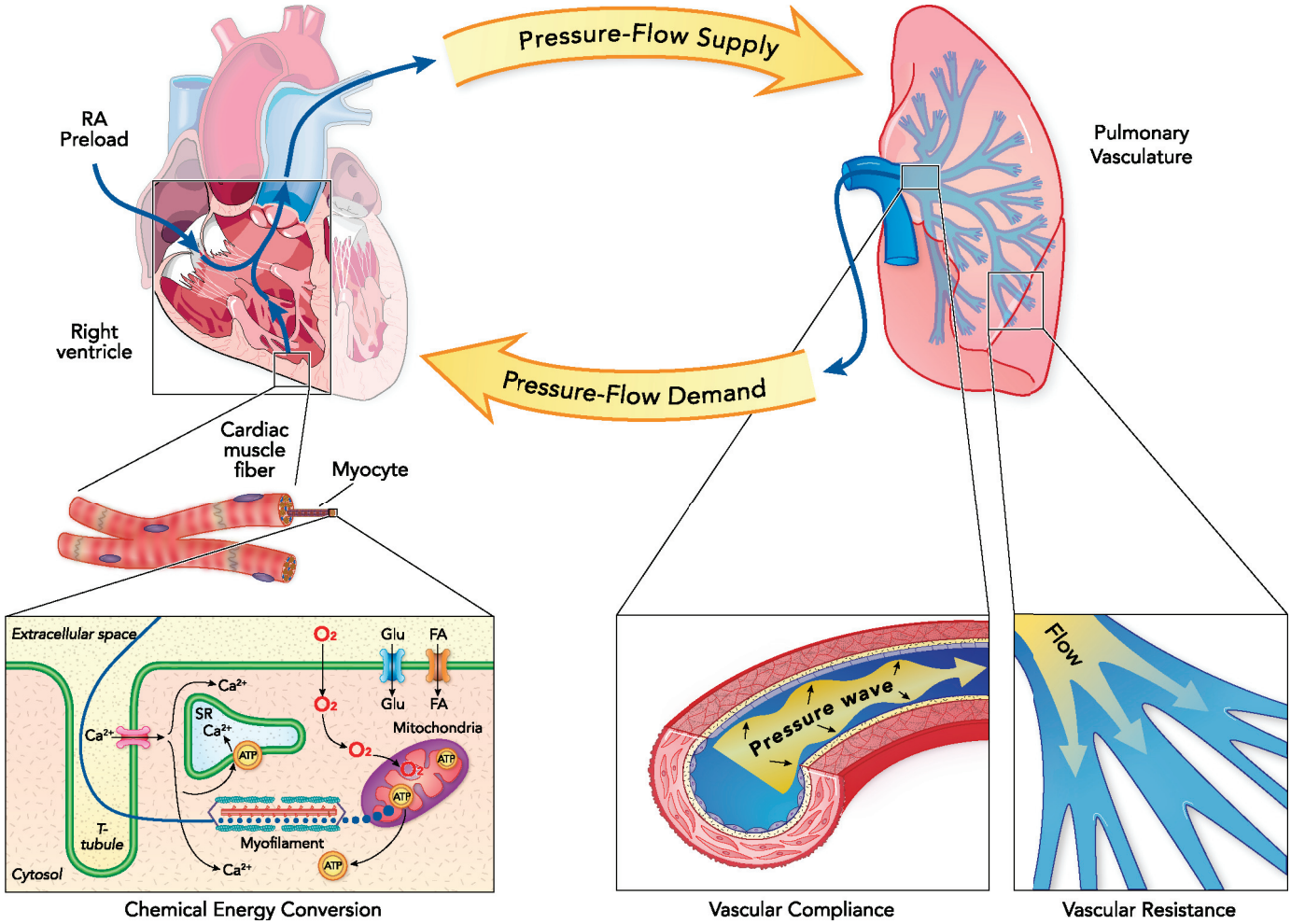

FIGURE 1. **Schematic of the relationship between supply and demand of right ventricular-pulmonary vascular unit**
Schematic of pressure and flow supply vs. demand showing the main contributors of right ventricular-pulmonary interactions including supply-side determinants: right ventricular dimensions and geometry, myocyte mechanics, and right ventricular preload; and demand-side determinants: pulmonary vascular compliance, which is dependent on transmission and modulation of pressure waves through large and small pulmonary arteries and pulmonary vascular resistance, which is dependent mostly on small arterial caliber and tone. Heart rate and left ventricular function are not shown.

that the RV supply is properly coupled to the demand of the pulmonary circulation (55) or that the RV-PV unit is operating with minimal energy cost (23, 66). However, some limitations in the application of this approach to RV-PV interactions exist. First, although E at end systole (E_{es}) is a good estimate of E_{max} in the LV, this is less true in the RV because of non-coincidence of end-ejection and end-systole (48). Second, RV P-V loops are frequently triangular in shape instead of square, which makes identification of the end-systolic point more difficult than in the LV (48, 62). Moreover, with increasing pulmonary vascular resistance due to PAH, the shape of RV P-V loops change: they become more square-shaped in mild PAH and then more trapezoidal in severe PAH (7, 53), which affects the calculation of E_{max}. Finally, V_0 varies more throughout the cardiac cycle in the RV than in the LV, such that the errors induced by assuming a constant V_0 are larger (48).

Approaches to examine RV-PV interactions other than P-V loop analysis do exist. One is pump function curves, which are traditionally built from measurements of the mean RV pressure that serves as a surrogate for PV demand, and stroke volume (SV) that serves as a surrogate for RV supply (86). There have been some limited pump function studies assessing RV function in PAH (58). However, the limitations of this approach, which include its sensitivity to changes in preload and neglect of pulsatile work components, have prevented it from being widely adopted in either clinical or preclinical studies.

A second alternative approach bases its estimation of PV demand on pulse-wave velocity and wave transit time in the heart, which are calculated through pulmonary vascular impedance (PVZ). Unlike pulmonary vascular resistance (PVR), which measures the opposition to steady flow, primarily determined by small-vessel resistance and a critical diagnostic criterion for PAH, PVZ measures the total opposition to flow through analysis of instantaneous arterial pressure and flow waves. PVZ provides the most comprehensive description of RV afterload, but its measurement is technically demanding (requiring simultaneously measured pressure and flow), and its computation is not standardized (to either frequency or time-domain analysis) (33, 80). Furthermore, PVZ does not enable straightforward assessment of PV demand coupling to RV supply.

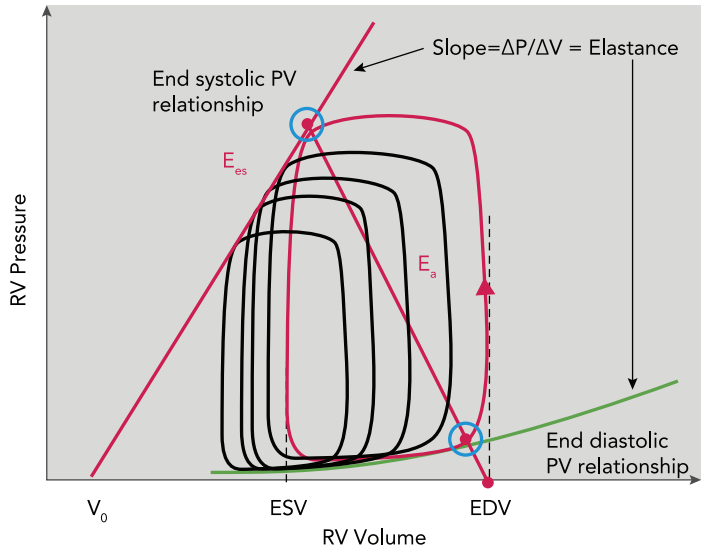

FIGURE 2. **Elastances derived from pressure-volume loops**
Pressure-volume loops showing the calculation of effective arterial elastance and end-systolic elastance by decreasing preload such as by inferior vena cava occlusion.

Application to Clinical Studies

Two main factors limit the assessment of RV-PV interactions via P-V loop analysis in the clinical setting. First, simultaneous pressure and volume measurements in the RV are difficult to obtain. Recently, an FDA P-V catheter approved for human use has been employed in clinical studies on the left ventricle (21, 60), but the non-cylindrical shape of the RV limits accuracy, especially at small volumes. Second, although it is possible to vary preload through inferior vena cava occlusions in animals, such maneuvers are not feasible in humans due to the increased risks of additional procedures and hemodynamic compromise. To overcome this limitation, both Hsu et al. and Tedford et al. had subjects perform Valsalva maneuvers to increase intrathoracic pressure during invasive right heart catheterization (RHC) with a P-V catheter, which successfully decreased preload in patients with idiopathic PAH and systemic sclerosis-associated PAH (32, 81). Nevertheless, the majority of clinical studies use approximations of P-V analysis with the methods summarized below.

The Single Beat Method

When P-V loops cannot be obtained instantaneously and simultaneously over multiple heartbeats with varying preload, the "single beat method," introduced by Sunagawa et al. for characterization of the left ventricle and left ventricular-systemic vascular coupling (56, 76, 79) and first applied to the RV-PV system by Brimioulle et al. (9) is often used. This method is based on a fitting of the early and late isovolumic contraction and relaxation ranges of the RV pressure waveform with a sine function (FIGURE 3A). The method assumes that ESPVR is the same in ejecting and non-ejecting beats and that the peak value of the sine function is the maximum pressure (P_{max}) that can be reached by a theoretical non-ejecting heartbeat. A straight line drawn from P_{max} to the RV

end-systolic pressure of the ejecting beat vs. the stroke volume permits a reasonably accurate estimation of $E_{es;sb}$ (which is within 15% of E_{es}; see Ref. 9) and is calculated as:

$$E_{es;sb} = \frac{P_{max} - P_{es}}{SV} \quad (1)$$

Although this method obviates the need to vary preload, simultaneously measuring pressure and volume remains an obstacle to widespread clinical application. As noted above, an FDA-approved conductance catheter enables collection of simultaneous P-V data, but this system is expensive and requires technical expertise. Two- and three-dimensional echocardiographic measurements of RV volume collected simultaneously with invasively measured PA pressure are possible (18, 31), but, given the noncylindrical shape of the RV, MRI-based volume measurements are preferred. MRI-derived RV volume measurements have been synchronized offline with RHC-derived RV pressure measurements (4, 44, 83), but recent advances in MRI catheterization (i.e., simultaneous MRI and RHC) allow acquisition of synchronous ventricular volume and pressure (65). To date, MRI catheterization has been used to create P-V loops in hypoplastic left heart syndrome (93); the future clinical impact of this approach may be considerable.

Since E_a is determined by a straight line from the end-systolic pressure point to the end-diastolic volume projected onto the volume axis, there is no loss of accuracy when it is calculated from a single beat as:

$$E_a = \frac{P_{es}}{SV} \quad (2)$$

In large animals, good agreement was found between the RV-PV coupling (VVC) estimated via the single-beat method $VVC_{sb} = E_{es;sb}/E_a$ and that calculated from multiple beats with preload reduction ($VVC = E_{es}/E_a$) (23, 44). Subsequently, the single-beat method has been used extensively in large animal (36–39, 59, 89) and in clinical studies (44, 58, 83, 88).

The Pressure Method

In the absence of RV volume measurements, the "pressure method" has been described to capture VVC based on parameters easy to obtain during a standard right heart catheterization. In this method, P_{max} is estimated from the sinusoidal extrapolation of the early systolic and diastolic portions of the RV pressure curve, the same as the method described above for the single-beat method, with P_{es} approximated by mPAP (13). This approximation requires two key assumptions: first that peak RV pressure is equal to P_{es}, and second that mPAP is an acceptable surrogate for peak RV pressure (8, 12, 13, 70). With this method, as detailed in (8, 70, 84):

$$VVC_p = \frac{P_{max}}{mPAP} - 1 \quad (3)$$

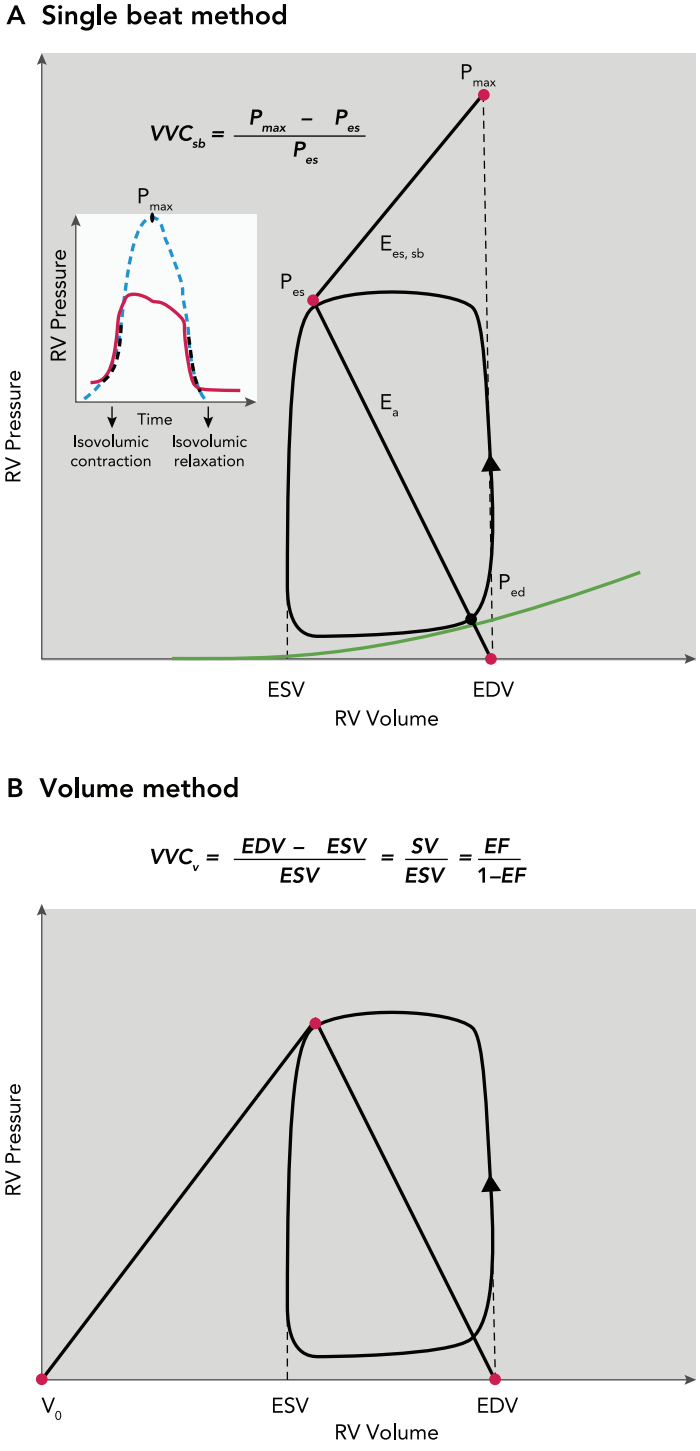

FIGURE 3. **Methods for approximating ventricular vascular coupling in clinical studies**
Comparison of the single-beat method (*A*) and the volume method (*B*) for the approximation of ventricular vascular coupling (VVC).

Table 1. *Studies evaluating RV-PV coupling in large animal models of pulmonary hypertension*

Model	Animal	E_a	E_{es}		VVC	References
Acute						
Pulmonary arterial banding	Dog, pig, goat	↑	↓		↓	35, 38, 39
Acute thromboembolism	Dog, goat	↑	Initial	Final	↓	23, 36, 37, 47
			↑	—		
Acute hypoxia	Dog,	↑	↑		—	20, 40, 63, 64
Endotoxic shock	Pigs	↑	Initial	Final	↓	45, 46
			↑	↓		
Acute RV ischemia	Pigs	↑	↓		↓	50
Chronic						
Over-pacing induced left heart failure	Dogs	↑	—		↓	59
Left PA ligation + sequential embolization	Pig	↑	↑		↓	27, 28

In general, the pressure method leads to higher values of coupling that are correlated with those from the single beat method (84).

The Volume Method

Alternatively, if RV volumes are available and RV pressures are not, the "volume method" has been described (70, 83, 84) in which:

$$VVC_v = \frac{SV}{ESV} \quad (4)$$

where ESV is end-systolic volume. Note that some authors use E_a/E_{es} to define coupling such that $VVC_v = ESV/SV$ (70, 83), but we strongly recommend E_{es}/E_a be used for consistency. Importantly, this approach assumes that *1*) RV end-systolic pressure (ESP) is equal to mPAP, *2*) the ESP-ESV relationship is linear, and *3*) V_0 equals zero (FIGURE 3B). As a consequence of these assumptions, this method tends to underestimate VVC. Moreover, as recently recognized by Vanderpool et al. (85), this metric is mathematically linked to the RV ejection fraction (EF):

$$VVC_v = \frac{SV}{ESV} = \frac{EF}{1 - EF} \quad (5)$$

and thus should not be more predictive of mortality than EF alone.

Acute Increases in PV Demand

An acute increase in RV supply in response to an acute increase in PV demand is a key component of adaptation to physiological stress, such as exercise, or pathological stress, such as pulmonary embolism. Preservation of RV-PV coupling in response to acute stressors has been investigated using acute hypoxia (20, 40, 63, 64) and acute thromboembolism (23, 36, 37, 47) (Table 1). In addition, the response of the RV to acute ischemia (50) and acute lung injury due to endotoxic shock have also been evaluated (45, 46). These studies provide key clinically relevant insights into RV function and adaptation in the setting of multiple models of increased demand, from mild to severe, that are summarized in Table 1.

Acute models of PAH also provide a time-efficient way to investigate the effect of drug therapies on RV-PV coupling (35, 37–40, 47, 50, 63, 64). As detailed in Table 2, various drugs have been investigated in large-animal models of acute pulmonary hypertension, including those that target the pulmonary vasculature (35, 63, 64), those that target the RV (37–39, 47, 50), and those that affect both (40). However, these studies typically assess only acute effects (10−120 min), thereby necessitating follow-up studies to determine whether any beneficial effects are sustained.

Insights Gained from Clinical Studies

Enabled by the novel technologies and the approximation methods described above, evaluation of VVC has provided important insights into the understanding of cardiopulmonary function, especially in PAH, in humans.

Kuehne et al. found that VVC_{sb} from non-simultaneous MRI and RHC was reduced in PAH subjects compared with controls, despite increased RV supply (44). McCabe found the same result in patients with chronic thromboembolic pulmonary hypertension compared with controls using conductance catheter-based VVC_{sb} measurements (49). In a retrospective analysis of 134 patients who underwent non-simultaneous RHC and MRI as work-up for PAH, Sanz et al. found that PAH subjects had significant elevations in E_a and $E_{es,p}$ compared with non-disease controls, as well as significant uncoupling as determined by decreased VVC_p (70).

Brewis et al. demonstrated a significant correlation between higher VVC_v and improved survival in

patients with PAH. Furthermore, patients in this study who had stable or improved VVC_v in response to therapy demonstrated improved survival (8). However, as noted above, given the mathematical links between VVC_v and EF, it is unclear how VVC_v adds value to prognoses.

Multiple studies have evaluated the correlation between VVC_{sb}, VVC_p, and VVC_v. These invasive and non-invasive estimates of VVC have been found to be highly correlative with *R* values ranging from 0.79 to 0.93 (70, 83, 84). Two studies with a total of over 150 patients between them demonstrated that VVC_v correlates with survival, whereas VVC_p does not (8, 84). Additional studies are required to address the question of whether VVC, quantified without additional simplifications, is a better predictor of mortality than VVC_{sb}, VVC_p, or VVC_v (or RV EF). If time-resolution limitations of MRI can be addressed, MRI catheterization with preload reduction by Valsalva could be used to conduct these studies. Otherwise, comprehensive hemodynamic studies in large-animal models as described below will be required.

Exercise as a Tool to Unmask Pathological Changes

Evaluation of the RV-PV response to exercise is increasingly a clinically applicable methodology that may unmask pathological changes not evident at rest. In healthy subjects, exercise increases heart rate and stroke volume (42, 54, 71), and the inability to do so is indicative of poor prognosis in PAH (5, 26, 72). From the perspective of RV-PV interactions, increased cardiac output, transformed by pulmonary vascular resistance and compliance, increases PV demand. Exercise can also decrease PVR (42, 43, 54, 71) and compliance (43, 71). Spruijt et al. studied both the RV and PV response to exercise, as well as their interactions. Control subjects demonstrated increased E_a and increased $E_{es;sb}$ with preservation of VVC_{sb}, which was in contrast to PAH subjects who demonstrated a significant decrease in VVC_{sb} (72). Bellofiore et al. demonstrated that PAH subjects with a lower VVC_{sb} at rest achieved a lower maximum exercise level and had limited reduction in pulmonary artery compliance during exercise (4). However, both of these studies were limited by low numbers of control subjects. In addition, the effects of increased heart rate on E_{es} and E_a were not taken into account. Accurate characterization of the normal response of the RV to exercise as well as interactions between the RV and PV during exercise, accounting for heart rate, are critical to evaluating the changes that occur in disease.

Physiological Insights from Large-Animal Studies

With appropriately chosen species, large-animal models have high fidelity to human cardiopulmonary physiology and pathology. Wauthy et al. evaluated the response to acute PAH caused by

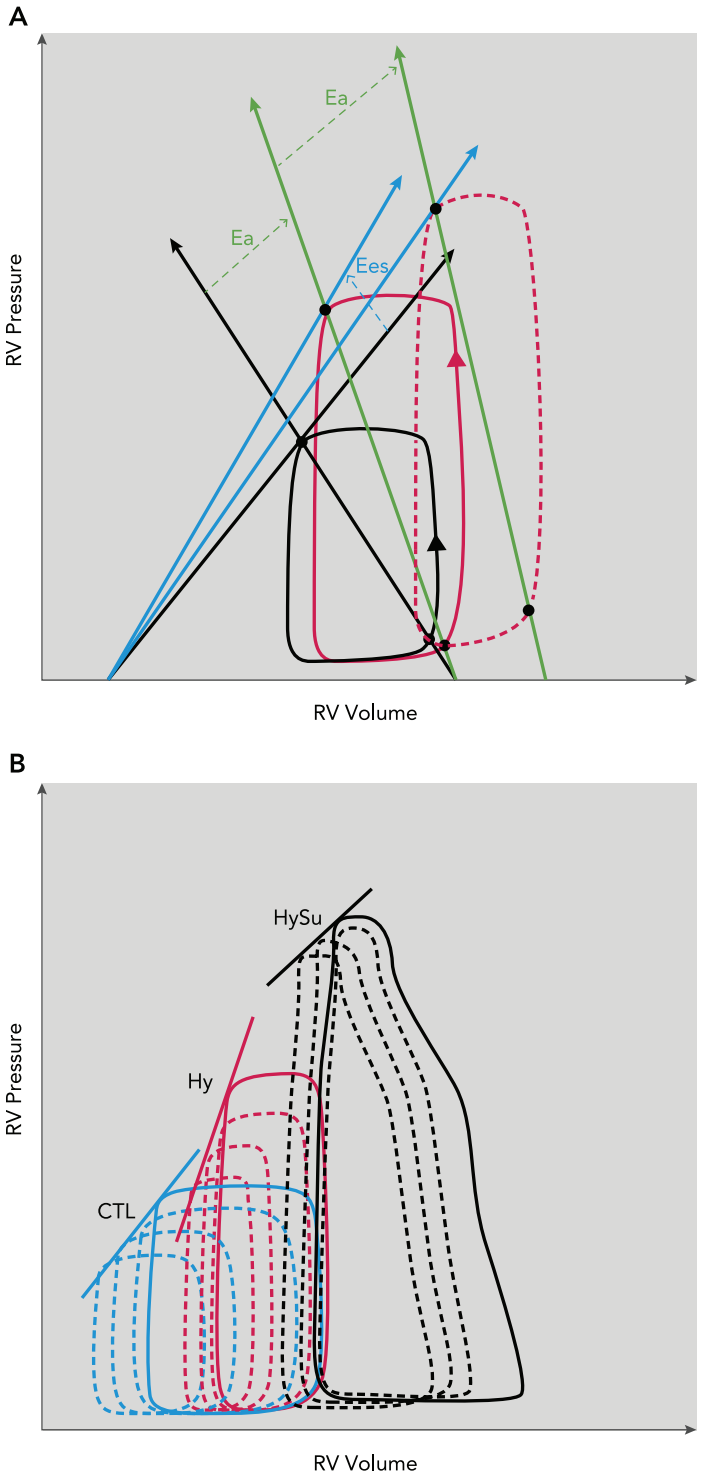

FIGURE 4. **Evolution of right ventricular response to PAH**
Changes in idealized pressure-volume loops with increases in afterload and RV dilatation (*A*) and representative pressure-volume loops (*B*) from mice with PAH and RV dilatation via chronic hypoxia (Hy) and hypoxia+sugen (HySu) acute decreases in preload to obtain E_{es}.

Table 2. *Studies evaluating the effect of pharmacological interventions on RV-PV coupling in large animal models of pulmonary hypertension*

Drug	Model	Animal	E_a	E_{es}	VVC	References
Vasoactive drugs						
Prostacyclins	Acute PA constriction, acute hypoxia	Dog, pig	↓	—/↓	↑/—	20, 35, 63, 64
Inhaled nitric oxide	Over-pacing induced left heart failure	Dog	—	—	—	59
Nitroprusside	Over-pacing induced left heart failure	Dog	—	—	—	59
Ionotropic drugs						
Milrinone	Over-pacing induced left heart failure	Dog	—	↑	↑	59
Norepinephrine	Acute PA constriction	Dog	↑	↑↑	↑	39
Dobutamine	Acute PA constriction	Dog	↑	↑↑	↑	38, 39
Vasopressin	Acute thromboembolism	Dog	↑	↓		47
Phenylephrine	Acute thromboembolism	Dogs	↑	—		47
Levosimedan	Acute PA constriction, ischemic RV failure, acute thromboembolism	Dog, pig	↓	↑	↑	37, 38, 50
Inhaled anesthetics						
Isoflurane, desflurane	Acute hypoxia and hyperoxia	Dog	↑	—	↓	40

pulmonary arterial banding (PAB), hypoxia, or thromboembolization in dogs, goats, and minipigs (89). Significant interspecies differences were found, with mPAP, E_a, and E_{es} at baseline increasing from dogs to goats to minipigs. Under baseline conditions, VVC was high in all species, and all species demonstrated similar responses to acute hypoxia, with progressive increases in both E_a and E_{es}, and no significant change in their ratio. Consistent with these findings, both dog and goats were demonstrated to have similar responses to both proximal PAB and acute thromboembolism (89), which suggests that both baseline RV-PV interactions and the adaptive response of the RV-PV unit to acute stress is conserved across species.

Several large-animal models of chronic PAH have been described, including monocrotaline (MCT)-induced PAH in dogs (14, 15, 29, 51), progressive pulmonary artery banding in pigs (2), pulmonary venous banding to induce postcapillary pulmonary hypertension in pigs (61), and a combination of chronic thromboembolism and proximal PA coiling in pigs (2). These studies demonstrate the feasibility of creating large-animal models of chronic pulmonary hypertension with the expected RV hypertrophy and decreased RV EF. However, RV-PV interactions were not quantified in these studies. Guihaire created a swine model of chronic PAH that combined left PA ligation and sequential embolization of the right lower pulmonary lobe (Table 1) (27, 28, 57). Chronic RV pressure overload was demonstrated by significantly increased mPAP after 6 wk, which was accompanied by increased E_a and E_{es}. Despite the increase in E_{es}, it was not sufficient to compensate for increased E_a, and consequently VVC decreased until perfusion was surgically restored to the left lung (27, 28). This chronic large-animal model provides useful insights into the adaptation of cardiopulmonary function to chronic PAH. However, it is resource intensive, requiring multiple surgeries as well as serial fluoroscopic-guided right heart catheterization for directed embolization.

Continued development of large-animal chronic PAH models with high fidelity to human disease and evaluation of these models with P-V loop analysis should provide insight into disease pathophysiology as well as for a platform for testing the safety and efficacy of novel therapies.

Mechanistic Insights from Small-Animal Studies

Although the hemodynamic changes that result from acute and chronic PAH in small animals may be less similar to the clinical situation than those of large animals, small-animal, especially mouse, studies enable use of sophisticated genetic tools that allow for evaluation of the molecular drivers of RV-PV uncoupling. Critical to the study of PAH in small-animal models is the ability to measure RV supply and PV demand.

Our group was the first to describe the use of P-V loop analysis to evaluate RV-PV function in rodents in 2010, adopting technologies and methodology previously used to evaluate left ventricular function. This study demonstrated the feasibility and utility of using an admittance catheter to measure P-V loops in anesthetized, open-chested mice before and during vena cava occlusion to alter preload, permitting the determination of E_{es}, E_a, and VVC as well as measurement of a multitude of metrics of both diastolic and systolic RV function. This initial study was done in a mouse model of chronic hypoxic pulmonary hypertension, which has the limitation that the PAH is reversible and

often mild (78) (FIGURE 4). Subsequently, we and others have used P-V loop analysis to characterize development of RV dysfunction in other rodent models of PAH (3, 16, 24, 25, 66, 87, 94).

A subsequent study from our group by Wang et al. examined the development of RV dysfunction and RV-PV uncoupling over time in a progressive model of hypoxia and SU5416 treatment (HySu exposure), a model of severe PAH that recapitulates the plexiform pulmonary vascular lesions seen in human PAH in rodents (1) (FIGURE 4); however, SU5416 may directly impact RV function since decreased angiogenesis and capillary density are associated with RV failure (6, 77). Both RV systolic pressure and E_a increased throughout the 28-day HySu exposure, whereas E_{es} only increased with HySu exposure up to 21 days, with no further increases seen between 21 and 28 days (with cardiac output increasing up to 14 days and then declining). Corresponding to these findings, VVC was initially preserved and even increased at 14 days of HySu exposure and then decreased consistent with uncoupling by 28 days. Through the rigorous investigation of RV function at multiple time points, this study demonstrates initial adaptation of the RV and subsequent maladaptation and failure after prolonged exposure to increased afterload (87).

Alaa et al. utilized P-V loop analysis to differentiate between PAH with preserved cardiac index (CI) and PAH with reduced CI in a MCT-induced model of PAH in rats (3). MCT has the advantages of causing severe PAH that recapitulates some of the pathological hallmarks of the disease in humans, such as distal smooth muscle hypertrophy, obliteration of small pulmonary arteriole lumens, and plexiform lesions (22, 91): however, it has the disadvantage of causing cardiac inflammation that may impair RV supply independent of increased RV demand (92). As expected, MCT-induced PAH led to increased RV systolic pressure, increased E_a, and increased E_{es} with decreased VVC. Interestingly, compared with PAH with preserved CI, PAH with reduced CI was associated with significantly higher E_a and E_{es}, but no significant difference in VVC. Moreover, although all MCT-treated animals demonstrated RV dilation, there was no difference in RV dilation between the preserved and reduced CI groups. This study, in which the inability to preserve CI was ultimately related to diastolic dysfunction (3), demonstrates that even the relatively comprehensive assessment of the cardiopulmonary unit afforded by P-V analysis can miss critical pathophysiological changes if only the standard metrics E_a, E_{es}, and VVC are evaluated.

As with large-animal studies, P-V analysis has been used to evaluate therapeutic interventions in rodent studies. Rungatscher et al. demonstrated *S*-nitroso human serum albumin (S-NO-HSA) treatment resulted in improvement in E_a, E_{es}, and VVC in a rat model of RV volume overload (66). Zeineh et al. showed a possible positive inotropic effect of iloprost, a prostacyclin, which resulted in increased VVC in a MCT rat model of PAH (94). De Man et al. demonstrated that β-blockade with bisoprolol delayed progression to RV failure and improved VVC in a MCT rat model of PAH (16). Despite promising results in small-animal studies, few of these findings are translatable into human therapies due the current limitations in large-animal studies for PAH and the fact that often therapies effective for small animals are not effective in large-animal models or human trials.

With the establishment of P-V loop analysis as a robust tool evaluating small-animal models of PAH, the impact of genetic modifications on RV-PV coupling has been investigated. Golob et al. demonstrated a benefit of genetically impaired collagen turnover on RV-PV coupling in a HySu model of PAH (25) and no effect from mitochondrial DNA mutation on RV-PV interactions (24) using P-V analysis. These studies provide important insights; however, more investigation is needed to understand the underlying molecular mechanisms that regulate RV function and RV-PV interactions.

P-V loop analysis in small-animal models provides a unique opportunity to study and understand the effects of molecular and cellular events leading to RV-PV uncoupling and RV failure. Future studies should help determine how modifications to cellular and extracellular structure impact RV-PV interactions, while providing a better understanding of the signaling pathways responsible for the transition from maintained RV function in the presence of increased afterload to RV failure.

Conclusions

The optimum management of PAH remains elusive. Evaluating the adequacy of hemodynamic interactions between the PV and RV through ventricular-vascular coupling is a powerful tool that should help in understanding disease development and progression as well as in the development, translation, and monitoring of novel therapies. Recommended areas of future work include:

1) Long-term studies on prognostic relevance of RV-PV interactions during both rest and exercise for PAH patients
2) Development of large-animal models that recapitulate pulmonary vascular disease phenotypes and enable validation of

pressure-only and volume-only approximations of VVC in healthy and diseased states

3) Consideration of RV-PV interactions in mechanistic studies to account for drivers of both RV supply and PV demand. ■

This work was supported by National Heart, Lung, and Blood Institute Grant R01 HL-086939 (N.C.C. and D.M.T.) and the Thoracic Surgery Foundation for Research and Education Nina Starr Braunwald Fellowship (J.L.P.).

No conflicts of interest, financial or otherwise, are declared by the author(s).

Author contributions: D.M.T., J.P., and N.C.C. interpreted results of experiments; D.M.T., J.P., and N.C.C. prepared figures; D.M.T. and J.P. drafted manuscript; D.M.T., J.P., and N.C.C. edited and revised manuscript; D.M.T., J.P., and N.C.C. approved final version of manuscript.

References

1. Abe K, Toba M, Alzoubi A, Ito M, Fagan KA, Cool CD, Voelkel NF, McMurtry IF, Oka M. Formation of plexiform lesions in experimental severe pulmonary arterial hypertension. *Circulation* 121: 2747–2754, 2010. doi:10.1161/CIRCULATIONAHA.109.927681.

2. Aguero J, Ishikawa K, Fish KM, Hammoudi N, Hadri L, Garcia-Alvarez A, Ibanez B, Fuster V, Hajjar RJ, Leopold JA. Combination proximal pulmonary artery coiling and distal embolization induces chronic elevations in pulmonary artery pressure in Swine. *PLoS One* 10: e0124526, 2015. doi:10.1371/journal.pone.0124526.

3. Alaa M, Abdellatif M, Tavares-Silva M, Oliveira-Pinto J, Lopes L, Leite S, Leite-Moreira AF, Lourenço AP. Right ventricular end-diastolic stiffness heralds right ventricular failure in monocrotaline-induced pulmonary hypertension. *Am J Physiol Heart Circ Physiol* 311: H1004–H1013, 2016. doi:10.1152/ajpheart.00202.2016.

4. Bellofiore A, Dinges E, Naeije R, Mkrdichian H, Beussink-Nelson L, Bailey M, Cuttica MJ, Sweis R, Runo JR, Keevil JG, Francois CJ, Shah SJ, Chesler NC. Reduced haemodynamic coupling and exercise are associated with vascular stiffening in pulmonary arterial hypertension. *Heart* 103: 421–427, 2016. doi:10.1136/heartjnl-2016-309906.

5. Blumberg FC, Arzt M, Lange T, Schroll S, Pfeifer M, Wensel R. Impact of right ventricular reserve on exercise capacity and survival in patients with pulmonary hypertension. *Eur J Heart Fail* 15: 771–775, 2013. doi:10.1093/eurjhf/hft044.

6. Bogaard HJ, Natarajan R, Henderson SC, Long CS, Kraskauskas D, Smithson L, Ockaili R, McCord JM, Voelkel NF. Chronic pulmonary artery pressure elevation is insufficient to explain right heart failure. *Circulation* 120: 1951–1960, 2009. doi:10.1161/CIRCULATIONAHA.109.883843.

7. Borgdorff MA, Koop AM, Bloks VW, Dickinson MG, Steendijk P, Sillje HH, van Wiechen MP, Berger RM, Bartelds B. Clinical symptoms of right ventricular failure in experimental chronic pressure load are associated with progressive diastolic dysfunction. *J Mol Cell Cardiol* 79: 244–253, 2015. doi:10.1016/j.yjmcc.2014.11.024.

8. Brewis MJ, Bellofiore A, Vanderpool RR, Chesler NC, Johnson MK, Naeije R, Peacock AJ. Imaging right ventricular function to predict outcome in pulmonary arterial hypertension. *Int J Cardiol* 218: 206–211, 2016. doi:10.1016/j.ijcard.2016.05.015.

9. Brimioulle S, Wauthy P, Ewalenko P, Rondelet B, Vermeulen F, Kerbaul F, Naeije R. Single-beat estimation of right ventricular end-systolic pressure-volume relationship. *Am J Physiol Heart Circ Physiol* 284: H1625–H1630, 2003. doi:10.1152/ajpheart.01023.2002.

10. Burkhoff D, Sagawa K. Ventricular efficiency predicted by an analytical model. *Am J Physiol* 250: R1021–R1027, 1986.

11. Burkhoff D, Sugiura S, Yue DT, Sagawa K. Contractility-dependent curvilinearity of end-systolic pressure-volume relations. *Am J Physiol Heart Circ Physiol* 252: H1218–H1227, 1987.

12. Chemla D, Castelain V, Zhu K, Papelier Y, Creuzé N, Hoette S, Parent F, Simonneau G, Humbert M, Herve P. Estimating right ventricular stroke work and the pulsatile work fraction in pulmonary hypertension. *Chest* 143: 1343–1350, 2013. doi:10.1378/chest.12-1880.

13. Chemla D, Hébert JL, Coirault C, Salmeron S, Zamani K, Lecarpentier Y. Matching dicrotic notch and mean pulmonary artery pressures: implications for effective arterial elastance. *Am J Physiol Heart Circ Physiol* 271: H1287–H1295, 1996.

14. Chen EP, Bittner HB, Craig DM, Davis RD Jr, Van Trigt P III. Pulmonary hemodynamics and blood flow characteristics in chronic pulmonary hypertension. *Ann Thorac Surg* 63: 806–813, 1997. doi:10.1016/S0003-4975(96)01258-1.

15. Chen EP, Bittner HB, Davis RD, Van Trigt P. Pulmonary vascular impedance and recipient chronic pulmonary hypertension following cardiac transplantation. *Chest* 112: 1622–1629, 1997. doi:10.1378/chest.112.6.1622.

16. de Man FS, Handoko ML, van Ballegoij JJ, Schalij I, Bogaards SJ, Postmus PE, van der Velden J, Westerhof N, Paulus WJ, Vonk-Noordegraaf A. Bisoprolol delays progression towards right heart failure in experimental pulmonary hypertension. *Circ Heart Fail* 5: 97–105, 2012. doi:10.1161/CIRCHEARTFAILURE.111.964494.

17. Dell'Italia LJ, Walsh RA. Application of a time varying elastance model to right ventricular performance in man. *Cardiovasc Res* 22: 864–874, 1988. doi:10.1093/cvr/22.12.864.

18. Ensing G, Seward J, Darragh R, Caldwell R. Feasibility of generating hemodynamic pressure curves from noninvasive Doppler echocardiographic signals. *J Am Coll Cardiol* 23: 434–442, 1994. doi:10.1016/0735-1097(94)90431-6.

19. Feneley MP, Gavaghan TP, Baron DW, Branson JA, Roy PR, Morgan JJ. Contribution of left ventricular contraction to the generation of right ventricular systolic pressure in the human heart. *Circulation* 71: 473–480, 1985. doi:10.1161/01.CIR.71.3.473.

20. Fesler P, Pagnamenta A, Rondelet B, Kerbaul F, Naeije R. Effects of sildenafil on hypoxic pulmonary vascular function in dogs. *J Appl Physiol (1985)* 101: 1085–1090, 2006. doi:10.1152/japplphysiol.00332.2006.

21. Gaemperli O, Biaggi P, Gugelmann R, Osranek M, Schreuder JJ, Bühler I, Sürder D, Lüscher TF, Felix C, Bettex D, Grünenfelder J, Corti R. Real-time left ventricular pressure-volume loops during percutaneous mitral valve repair with the MitraClip system. *Circulation* 127: 1018–1027, 2013. doi:10.1161/CIRCULATIONAHA.112.135061.

22. Ghodsi F, Will JA. Changes in pulmonary structure and function induced by monocrotaline intoxication. *Am J Physiol Heart Circ Physiol* 240: H149–H155, 1981.

23. Ghuysen A, Lambermont B, Kolh P, Tchana-Sato V, Magis D, Gerard P, Mommens V, Janssen N, Desaive T, D'Orio V. Alteration of right ventricular-pulmonary vascular coupling in a porcine model of progressive pressure overloading. *Shock* 29: 197–204, 2008.

24. Golob MJ, Tian L, Wang Z, Zimmerman TA, Caneba CA, Hacker TA, Song G, Chesler NC. Mitochondria DNA mutations cause sex-dependent development of hypertension and alterations in cardiovascular function. *J Biomech* 48: 405–412, 2015. doi:10.1016/j.jbiomech.2014.12.044.

25. Golob MJ, Wang Z, Prostrollo AJ, Hacker TA, Chesler NC. Limiting collagen turnover via collagenase-resistance attenuates right ventricular dysfunction and fibrosis in pulmonary arterial hypertension. *Physiol Rep* 4: e12815, 2016. doi:10.14814/phy2.12815.

26. Grünig E, Tiede H, Enyimayew EO, Ehlken N, Seyfarth H-J, Bossone E, D'Andrea A, Naeije R, Olschewski H, Ulrich S, Nagel C, Halank M, Fischer C. Assessment and prognostic relevance of right ventricular contractile reserve in patients with severe pulmonary hypertension. *Circulation* 128: 2005–2015, 2013. doi:10.1161/CIRCULATIONAHA.113.001573.

27. Guihaire J, Haddad F, Boulate D, Capderou A, Decante B, Flécher E, Eddahibi S, Dorfmüller P, Hervé P, Humbert M, Verhoye JP, Dartevelle P, Mercier O, Fadel E. Right ventricular plasticity in a porcine model of chronic pressure overload. *J Heart Lung Transplant* 33: 194–202, 2014. doi:10.1016/j.healun.2013.10.026.

28. Guihaire J, Haddad F, Boulate D, Decante B, Denault AY, Wu J, Hervé P, Humbert M, Dartevelle P, Verhoye JP, Mercier O, Fadel E. Non-invasive indices of right ventricular function are markers of ventricular-arterial coupling rather than ventricular contractility: insights from a porcine model of chronic pressure overload. *Eur Heart J Cardiovasc Imaging* 14: 1140–1149, 2013. doi:10.1093/ehjci/jet092.

29. Gust R, Schuster DP. Vascular remodeling in experimentally induced subacute canine pulmonary hypertension. *Exp Lung Res* 27: 1–12, 2001. doi:10.1080/019021401459734.

30. Haddad F, Hunt SA, Rosenthal DN, Murphy DJ. Right ventricular function in cardiovascular disease, part I: Anatomy, physiology, aging, and functional assessment of the right ventricle. *Circulation* 117: 1436–1448, 2008. doi:10.1161/CIRCULATIONAHA.107.653576.

31. Hemnes AR, Forfia PR, Champion HC. Assessment of pulmonary vasculature and right heart by invasive haemodynamics and echocardiography. *Int J Clin Pract Suppl* 63: 4–19, 2009. doi:10.1111/j.1742-1241.2009.02110.x.

32. Hsu S, Houston BA, Tampakakis E, Bacher AC, Rhodes PS, Mathai SC, Damico RL, Kolb TM, Hummers LK, Shah AA, McMahan Z, Corona-Villalobos CP, Zimmerman SL, Wigley FM, Hassoun PM, Kass DA, Tedford RJ. Right ventricular functional reserve in pulmonary arterial hypertension. *Circulation* 133: 2413–2422, 2016. doi:10.1161/CIRCULATIONAHA.116.022082.

33. Huez S, Brimioulle S, Naeije R, Vachiéry JL. Feasibility of routine pulmonary arterial impedance measurements in pulmonary hypertension. *Chest* 125: 2121–2128, 2004. doi:10.1378/chest.125.6.2121.

34. Kass DA, Beyar R, Lankford E, Heard M, Maughan WL, Sagawa K. Influence of contractile state on curvilinearity of in situ end-systolic pressure-volume relations. *Circulation* 79: 167–178, 1989. doi:10.1161/01.CIR.79.1.167.

35. Kerbaul F, Brimioulle S, Rondelet B, Dewachter C, Hubloue I, Naeije R. How prostacyclin improves cardiac output in right heart failure in conjunction with pulmonary hypertension. *Am J Respir Crit Care Med* 175: 846–850, 2007. doi:10.1164/rccm.200611-1615OC.

36. Kerbaul F, By Y, Gariboldi V, Mekkaoui C, Fesler P, Collart F, Brimioulle S, Jammes Y, Ruf J, Guieu R. Acute pulmonary embolism decreases adenosine plasma levels in anesthetized pigs. *ISRN Cardiol* 2011: 750301, 2011. doi:10.5402/2011/750301.

37. Kerbaul F, Gariboldi V, Giorgi R, Mekkaoui C, Guieu R, Fesler P, Gouin F, Brimioulle S, Collart F. Effects of levosimendan on acute pulmonary embolism-induced right ventricular failure. *Crit Care Med* 35: 1948–1954, 2007. doi:10.1097/01.CCM.0000275266.33910.8D.

38. Kerbaul F, Rondelet B, Demester JP, Fesler P, Huez S, Naeije R, Brimioulle S. Effects of levosimendan versus dobutamine on pressure load-induced right ventricular failure. *Crit Care Med* 34: 2814–2819, 2006. doi:10.1097/01.CCM.0000242157.19347.50.

39. Kerbaul F, Rondelet B, Motte S, Fesler P, Hubloue I, Ewalenko P, Naeije R, Brimioulle S. Effects of norepinephrine and dobutamine on pressure load-induced right ventricular failure. *Crit Care Med* 32: 1035–1040, 2004. doi:10.1097/01.CCM.0000120052.77953.07.

40. Kerbaul F, Rondelet B, Motte S, Fesler P, Hubloue I, Ewalenko P, Naeije R, Brimioulle S. Isoflurane and desflurane impair right ventricular-pulmonary arterial coupling in dogs. *Anesthesiology* 101: 1357–1362, 2004. doi:10.1097/00000542-200412000-00016.

41. Khalafbeigui F, Suga H, Sagawa K. Left ventricular systolic pressure-volume area correlates with oxygen consumption. *Am J Physiol* 237: H566–H569, 1979.

42. Kovacs G, Berghold A, Scheidl S, Olschewski H. Pulmonary arterial pressure during rest and exercise in healthy subjects: a systematic review. *Eur Respir J* 34: 888–894, 2009. doi:10.1183/09031936.00145608.

43. Kovacs G, Olschewski A, Berghold A, Olschewski H. Pulmonary vascular resistances during exercise in normal subjects: a systematic review. *Eur Respir J* 39: 319–328, 2012. doi:10.1183/09031936.00008611.

44. Kuehne T, Yilmaz S, Steendijk P, Moore P, Groenink M, Saaed M, Weber O, Higgins CB, Ewert P, Fleck E, Nagel E, Schulze-Neick I, Lange P. Magnetic resonance imaging analysis of right ventricular pressure-volume loops: in vivo validation and clinical application in patients with pulmonary hypertension. *Circulation* 110: 2010–2016, 2004. doi:10.1161/01.CIR.0000143138.02493.DD.

45. Lambermont B, Delanaye P, Dogné JM, Ghuysen A, Janssen N, Dubois B, Desaive T, Kolh P, D'Orio V, Krzesinski JM. Large-pore membrane hemofiltration increases cytokine clearance and improves right ventricular-vascular coupling during endotoxic shock in pigs. *Artif Organs* 30: 560–564, 2006. doi:10.1111/j.1525-1594.2006.00260.x.

46. Lambermont B, Ghuysen A, Kolh P, Tchana-Sato V, Segers P, Gérard P, Morimont P, Magis D, Dogné JM, Masereel B, D'Orio V. Effects of endotoxic shock on right ventricular systolic function and mechanical efficiency. *Cardiovasc Res* 59: 412–418, 2003. doi:10.1016/S0008-6363(03)00368-7.

47. Leather HA, Segers P, Berends N, Vandermeersch E, Wouters PF. Effects of vasopressin on right ventricular function in an experimental model of acute pulmonary hypertension. *Crit Care Med* 30: 2548–2552, 2002. doi:10.1097/00003246-200211000-00024.

48. Maughan WL, Shoukas AA, Sagawa K, Weisfeldt ML. Instantaneous pressure-volume relationship of the canine right ventricle. *Circ Res* 44: 309–315, 1979. doi:10.1161/01.RES.44.3.309.

49. McCabe C, White PA, Hoole SP, Axell RG, Priest AN, Gopalan D, Taboada D, MacKenzie Ross R, Morrell NW, Shapiro LM, Pepke-Zaba J. Right ventricular dysfunction in chronic thromboembolic obstruction of the pulmonary artery: a pressure-volume study using the conductance catheter. *J Appl Physiol (1985)* 116: 355–363, 2014. doi:10.1152/japplphysiol.01123.2013.

50. Missant C, Rex S, Segers P, Wouters PF. Levosimendan improves right ventriculovascular coupling in a porcine model of right ventricular dysfunction. *Crit Care Med* 35: 707–715, 2007. doi:10.1097/01.CCM.0000257326.96342.57.

51. Moon MR, Aziz A, Lee AM, Moon CJ, Okada S, Kanter EM, Yamada KA. Differential calcium handling in two canine models of right ventricular pressure overload. *J Surg Res* 178: 554–562, 2012. doi:10.1016/j.jss.2012.04.066.

52. Murakami M, Mikuniya A, Suto N, Okubo T, Shinozaki N, Okumura K. Effects of cardiac sympathetic nerve stimulation on the left ventricular end-systolic pressure-volume relationship and plasma norepinephrine dynamics in dogs. *Jpn Circ J* 61: 864–871, 1997. doi:10.1253/jcj.61.864.

53. Naeije R. Assessment of right ventricular function in pulmonary hypertension. *Curr Hypertens Rep* 17: 35, 2015. doi:10.1007/s11906-015-0546-0.

54. Naeije R, Chesler N. Pulmonary circulation at exercise. *Compr Physiol* 2: 711–741, 2012.

55. Naeije R, Vizza D. Current perspectives modern hemodynamic evaluation of the pulmonary circulation. Application to pulmonary arterial hypertension and embolic pulmonary hypertension. *Ital Heart J* 6: 784–788, 2005.

56. Nakamoto T, Cheng CP, Santamore WP, Iizuka M. Estimation of left ventricular elastance without altering preload or afterload in the conscious dog. *Cardiovasc Res* 27: 868–873, 1993. doi:10.1093/cvr/27.5.868.

57. Noly PE, Guihaire J, Coblence M, Dorfmüller P, Fadel E, Mercier O. Chronic thromboembolic pulmonary hypertension and assessment of right ventricular function in the piglet. *J Vis Exp* 105: e53133, 2015.

58. Overbeek MJ, Lankhaar JW, Westerhof N, Voskuyl AE, Boonstra A, Bronzwaer JG, Marques KM, Smit EF, Dijkmans BA, Vonk-Noordegraaf A. Right ventricular contractility in systemic sclerosis-associated and idiopathic pulmonary arterial hypertension. *Eur Respir J* 31: 1160–1166, 2008. doi:10.1183/09031936.00135407.

59. Pagnamenta A, Dewachter C, McEntee K, Fesler P, Brimioulle S, Naeije R. Early right ventriculo-arterial uncoupling in borderline pulmonary hypertension on experimental heart failure. *J Appl Physiol (1985)* 109: 1080–1085, 2010. doi:10.1152/japplphysiol.00467.2010.

60. Pappone C, Calović Ž, Vicedomini G, Cuko A, McSpadden LC, Ryu K, Romano E, Saviano M, Baldi M, Pappone A, Ciaccio C, Giannelli L, Ionescu B, Petretta A, Vitale R, Fundaliotis A, Tavazzi L, Santinelli V. Multipoint left ventricular pacing improves acute hemodynamic response assessed with pressure-volume loops in cardiac resynchronization therapy patients. *Heart Rhythm* 11: 394–401, 2014. doi:10.1016/j.hrthm.2013.11.023.

61. Pereda D, García-Alvarez A, Sánchez-Quintana D, Nuño M, Fernández-Friera L, Fernández-Jiménez R, García-Ruíz JM, Sandoval E, Aguero J, Castellá M, Hajjar RJ, Fuster V, Ibáñez B. Swine model of chronic postcapillary pulmonary hypertension with right ventricular remodeling: long-term characterization by cardiac catheterization, magnetic resonance, and pathology. *J Cardiovasc Transl Res* 7: 494–506, 2014. doi:10.1007/s12265-014-9564-6.

62. Redington AN, Gray HH, Hodson ME, Rigby ML, Oldershaw PJ. Characterisation of the normal right ventricular pressure-volume relation by biplane angiography and simultaneous micromanometer pressure measurements. *Br Heart J* 59: 23–30, 1988. doi:10.1136/hrt.59.1.23.

63. Rex S, Missant C, Claus P, Buhre W, Wouters PF. Effects of inhaled iloprost on right ventricular contractility, right ventriculo-vascular coupling and ventricular interdependence: a randomized placebo-controlled trial in an experimental model of acute pulmonary hypertension. *Crit Care* 12: R113, 2008. doi:10.1186/cc7005.

64. Rex S, Missant C, Segers P, Rossaint R, Wouters PF. Epoprostenol treatment of acute pulmonary hypertension is associated with a paradoxical decrease in right ventricular contractility. *Intensive Care Med* 34: 179–189, 2008. doi:10.1007/s00134-007-0831-8.

65. Rogers T, Ratnayaka K, Lederman RJ. MRI catheterization in cardiopulmonary disease. *Chest* 145: 30–36, 2014. doi:10.1378/chest.13-1759.

66. Rungatscher A, Hallström S, Linardi D, Milani E, Gasser H, Podesser BK, Scarabelli TM, Luciani GB, Faggian G. S-nitroso human serum albumin attenuates pulmonary hypertension, improves right ventricular-arterial coupling, and reduces oxidative stress in a chronic right ventricle volume overload model. *J Heart Lung Transplant* 34: 479–488, 2015. doi:10.1016/j.healun.2014.09.041.

67. Sagawa K. *Cardiac Contraction and the Pressure-Volume Relationship*. Oxford, UK: Oxford Univ. Press, 1988.

68. Sagawa K. The end-systolic pressure-volume relation of the ventricle: definition, modifications and clinical use. *Circulation* 63: 1223–1227, 1981. doi:10.1161/01.CIR.63.6.1223.

69. Santamore WP, Dell'Italia LJ. Ventricular interdependence: significant left ventricular contributions to right ventricular systolic function. *Prog Cardiovasc Dis* 40: 289–308, 1998. doi:10.1016/S0033-0620(98)80049-2.

70. Sanz J, García-Alvarez A, Fernández-Friera L, Nair A, Mirelis JG, Sawit ST, Pinney S, Fuster V. Right ventriculo-arterial coupling in pulmonary hypertension: a magnetic resonance study. *Heart* 98: 238–243, 2012. doi:10.1136/heartjnl-2011-300462.

71. Slife DM, Latham RD, Sipkema P, Westerhof N. Pulmonary arterial compliance at rest and exercise in normal humans. *Am J Physiol Heart Circ Physiol* 258: H1823–H1828, 1990.

72. Spruijt OA, de Man FS, Groepenhoff H, Oosterveer F, Westerhof N, Vonk-Noordegraaf A, Bogaard HJ. The effects of exercise on right ventricular contractility and right ventricular-arterial coupling in pulmonary hypertension. *Am J Respir Crit Care Med* 191: 1050–1057, 2015. doi:10.1164/rccm.201412-2271OC.

73. Sunagawa K, Maughan WL, Burkhoff D, Sagawa K. Left ventricular interaction with arterial load studied in isolated canine ventricle. *Am J Physiol Heart Circ Physiol* 245: H773–H780, 1983.

74. Sunagawa K, Maughan WL, Friesinger G, Guzman P, Chang MS, Sagawa K. Effects of coronary arterial pressure on left ventricular end-systolic pressure-volume relation of isolated canine heart. *Circ Res* 50: 727–734, 1982. doi:10.1161/01.RES.50.5.727.

75. Sunagawa K, Maughan WL, Sagawa K. Optimal arterial resistance for the maximal stroke work studied in isolated canine left ventricle. *Circ Res* 56: 586–595, 1985. doi:10.1161/01.RES.56.4.586.

76. Sunagawa K, Yamada A, Senda Y, Kikuchi Y, Nakamura M, Shibahara T, Nose Y. Estimation of the hydromotive source pressure from ejecting beats of the left ventricle. *IEEE Trans Biomed Eng* 27: 299–305, 1980. doi:10.1109/TBME.1980.326737.

77. Sutendra G, Dromparis P, Paulin R, Zervopoulos S, Haromy A, Nagendran J, Michelakis ED. A metabolic remodeling in right ventricular hypertrophy is associated with decreased angiogenesis and a transition from a compensated to a decompensated state in pulmonary hypertension. *J Mol Med (Berl)* 91: 1315–1327, 2013. doi:10.1007/s00109-013-1059-4.

78. Tabima DM, Hacker TA, Chesler NC. Measuring right ventricular function in the normal and hypertensive mouse hearts using admittance-derived pressure-volume loops. *Am J Physiol Heart Circ Physiol* 299: H2069–H2075, 2010. doi:10.1152/ajpheart.00805.2010.

79. Takeuchi M, Igarashi Y, Tomimoto S, Odake M, Hayashi T, Tsukamoto T, Hata K, Takaoka H, Fukuzaki H. Single-beat estimation of the slope of the end-systolic pressure-volume relation in the human left ventricle. *Circulation* 83: 202–212, 1991. doi:10.1161/01.CIR.83.1.202.

80. Tedford RJ. Determinants of right ventricular afterload (2013 Grover Conference series). *Pulm Circ* 4: 211–219, 2014. doi:10.1086/676020.

81. Tedford RJ, Mudd JO, Girgis RE, Mathai SC, Zaiman AL, Housten-Harris T, Boyce D, Kelemen BW, Bacher AC, Shah AA, Hummers LK, Wigley FM, Russell SD, Saggar R, Saggar R, Maughan WL, Hassoun PM, Kass DA. Right ventricular dysfunction in systemic sclerosis-associated pulmonary arterial hypertension. *Circ Heart Fail* 6: 953–963, 2013. doi:10.1161/CIRCHEARTFAILURE.112.000008.

82. Thenappan T, Shah SJ, Rich S, Tian L, Archer SL, Gomberg-Maitland M. Survival in pulmonary arterial hypertension: a reappraisal of the NIH risk stratification equation. *Eur Respir J* 35: 1079–1087, 2010. doi:10.1183/09031936.00072709.

83. Truong U, Patel S, Kheyfets V, Dunning J, Fonseca B, Barker AJ, Ivy D, Shandas R, Hunter K. Non-invasive determination by cardiovascular magnetic resonance of right ventricular-vascular coupling in children and adolescents with pulmonary hypertension. *J Cardiovasc Magn Reson* 17: 81, 2015. doi:10.1186/s12968-015-0186-1.

84. Vanderpool RR, Pinsky MR, Naeije R, Deible C, Kosaraju V, Bunner C, Mathier MA, Lacomis J, Champion HC, Simon MA. RV-pulmonary arterial coupling predicts outcome in patients referred for pulmonary hypertension. *Heart* 101: 37–43, 2015. doi:10.1136/heartjnl-2014-306142.

85. Vanderpool RR, Rischard F, Naeije R, Hunter K, Simon MA. Simple functional imaging of the right ventricle in pulmonary hypertension: can right ventricular ejection fraction be improved? *Int J Cardiol* 223: 93–94, 2016. doi:10.1016/j.ijcard.2016.08.138.

86. Vonk-Noordegraaf A, Westerhof N. Describing right ventricular function. *Eur Respir J* 41: 1419–1423, 2013. doi:10.1183/09031936.00160712.

87. Wang Z, Schreier DA, Hacker TA, Chesler NC. Progressive right ventricular functional and structural changes in a mouse model of pulmonary arterial hypertension. *Physiol Rep* 1: e00184, 2013. doi:10.1002/phy2.184.

88. Wauthy P, Naeije R, Brimioulle S. Left and right ventriculo-arterial coupling in a patient with congenitally corrected transposition. *Cardiol Young* 15: 647–649, 2005. doi:10.1017/S1047951105001848.

89. Wauthy P, Pagnamenta A, Vassalli F, Naeije R, Brimioulle S. Right ventricular adaptation to pulmonary hypertension: an interspecies comparison. *Am J Physiol Heart Circ Physiol* 286: H1441–H1447, 2004. doi:10.1152/ajpheart.00640.2003.

90. Westerhof N, Stergiopulos N, Nobel MIM. *Snapshots of Hemodynamics: An Aid for Clinical Research and Graduate Education*. New York: Springer, 2010, p. 77–87. doi:10.1007/978-1-4419-6363-5_13.

91. White RJ, Meoli DF, Swarthout RF, Kallop DY, Galaria II, Harvey JL, Miller CM, Blaxall BC, Hall CM, Pierce RA, Cool CD, Taubman MB. Plexiform-like lesions and increased tissue factor expression in a rat model of severe pulmonary arterial hypertension. *Am J Physiol Lung Cell Mol Physiol* 293: L583–L590, 2007. doi:10.1152/ajplung.00321.2006.

92. Wilson DW, Segall HJ, Pan LC, Dunston SK. Progressive inflammatory and structural changes in the pulmonary vasculature of monocrotaline-treated rats. *Microvasc Res* 38: 57–80, 1989. doi:10.1016/0026-2862(89)90017-4.

93. Wong J, Pushparajah K, de Vecchi A, Ruijsink B, Greil GF, Hussain T, Razavi R. Pressure-volume loop-derived cardiac indices during dobutamine stress: a step towards understanding limitations in cardiac output in children with hypoplastic left heart syndrome. *Int J Cardiol* 230: 439–446, 2017. doi:10.1016/j.ijcard.2016.12.087.

94. Zeineh NS, Bachman TN, El-Haddad H, Champion HC. Effects of acute intravenous iloprost on right ventricular hemodynamics in rats with chronic pulmonary hypertension. *Pulm Circ* 4: 612–618, 2014. doi:10.1086/677358.

95. Zhong L, Ghista DN, Ng EY, Lim ST. Passive and active ventricular elastances of the left ventricle. *Biomed Eng Online* 4: 10, 2005. doi:10.1186/1475-925X-4-10.